ON THE SELF-SIMILAR DIFFRACTION OF A WEAK SHOCK INTO AN EXPANSION WAVEFRONT

JOHN K. HUNTER* AND ALLEN M. TESDALL†

Abstract. We study an asymptotic problem that describes the diffraction of a weak, self-similar shock near a point where its shock strength approaches zero and the shock turns continuously into an expansion wavefront. An example arises in the reflection of a weak shock off a semi-infinite screen. The asymptotic problem consists of the unsteady transonic small disturbance equation with suitable matching conditions. We obtain numerical solutions of this problem, which show that the shock diffracts nonlinearly into the expansion region. We also solve numerically a related half-space problem with a "soft" boundary, which shows a complex reflection pattern similar to one that occurs in the Guderley Mach reflection of weak shocks.

Key words. Shock diffraction, hyperbolic conservation laws, two-dimensional Riemann problems, unsteady transonic small disturbance equation.

AMS subject classifications. 65M06, 35L65, 76L05

1. Introduction.

Suppose that a weak plane shock wave of constant strength hits a semi-infinite, rigid screen at normal incidence (see Figure 1). This problem is self-similar, or pseudo-steady, and the solution depends only on $(x/t, y/t)$ where (x, y) are Cartesian spatial coordinates and $t > 0$ is time. (We ignore any complications associated with the viscous separation of a vortex sheet from the edge of the screen.)

The incident shock diffracts around the screen and a cylindrical diffracted expansion wavefront generated from the edge of the screen propagates behind it. Similarly, the reflected shock diffracts past the screen, and the diffracted reflected shock meets the diffracted expansion wave near the point S. Our interest is in understanding the local structure of self-similar solutions of the compressible Euler equations near a point such as S where the shock strength approaches zero and the wave changes continuously from a shock into an expansion.

The method of matched asymptotic expansions shows that, in the weak shock limit, the solution near S is described asymptotically by a self-similar solution of the unsteady transonic small disturbance equation (UTSDE) in $t > 0$,

$$\begin{aligned} &u_t + \left(\frac{1}{2}u^2\right)_x + v_y = 0, \\ &u_y - v_x = 0, \end{aligned} \tag{1.1}$$

with the matching, or initial condition, that

$$\begin{aligned} &u \sim \alpha \frac{y}{t}\sqrt{-\left(\frac{x}{t} + \frac{y^2}{4t^2}\right)} \qquad \text{as } \frac{x}{t} + \frac{y^2}{4t^2} \to -\infty, \\ &u = 0 \qquad \text{for } \frac{x}{t} + \frac{y^2}{4t^2} \text{ sufficiently large and positive.} \end{aligned} \tag{1.2}$$

*Department of Mathematics, University of California at Davis, Davis, CA 95616 (jkhunter@ucdavis.edu). This author's research was partially supported by National Science Foundation grant DMS-1009538.

†Department of Mathematics, College of Staten Island, City University of New York, Staten Island, NY 10314 (allen.tesdall@csi.cuny.edu). This author's research was supported by Department of Energy grant DE-SC0001378 and Research Foundation of CUNY grant 60145-39 40.

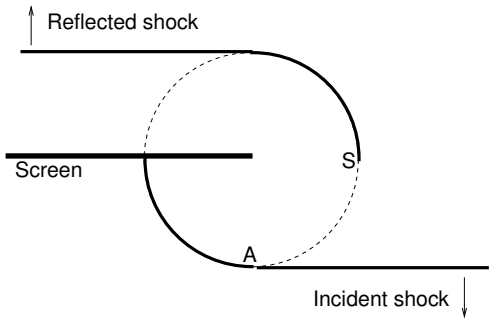

FIG. 1. *A weak shock at normal incidence to a screen. Solid lines are shocks; dotted lines are expansion wavefronts.*

In (1.2), the small positive parameter α measures the strength of the wave, and it cannot be removed by a rescaling. The matching data (1.2) corresponds to a self-similar radial sound wave that changes continuously from a compression in $y > 0$ to an expansion in $y < 0$.

The spatial variables (x, y) in (1.1)–(1.2) are suitably defined "inner" spatial variables about S, rather the original spatial variables. The x-variable increases across the wavefront, and the y-variable increases along the wavefront. The dependent variables (u, v) are proportional to the (x, y) velocity perturbations, and the pressure perturbation is proportional to u. We summarize the derivation of the UTSDE and the definitions of the variables in the Appendix.

In Section 8.1, we show numerical solutions of (1.1)–(1.2) for several different small values of α. A shock wave forms by compression in $y > 0$ and diffracts into the lower half space $y < 0$, where it dies out at some point and is continued by an expansion wavefront. The shock appears to diffract by an angle that is of the order α as $\alpha \to 0^+$; specifically, we find numerically that it dies out at a point with $y/t \sim -c\alpha$, where $c \approx 5.75$. This point appears from our numerical solutions to be on the sonic line where the self-similar form of (1.1) changes type, and not inside the supersonic region. The disappearance of a diffracting shock at a sonic point differs from the formation of shocks in two-dimensional Riemann problems and transonic flows that is caused by the focusing of characteristics reflected off a sonic line. Such shocks typically form at supersonic points [14]. See [10] for an analysis of related problems.

The weakly nonlinear asymptotics for the solution near a point such as S is subtle. A straightforward dominant balance argument based on transonic scaling and matching with the global linearized solution is not sufficient to determine the size of the region near S where nonlinearity becomes important. Related to this difficulty is the fact that, as we show in Section 5, the UTSDE and the matching condition (1.1)–(1.2) are self-similar in the similarity variables $(x/t, y/t)$. Thus, remarkably, this problem possesses a second self-similarity with respect to the original self-similar variables. The second self-similarity appears to be broken, however, by the difference between the conditions required at a shock and an expansion wavefront, so that the full solution is not self-similar. We do not carry out a complete analysis of these issues here, but we obtain numerical solutions of (1.1)–(1.2).

The phenomenon of a shock that propagates into a constant state and diffracts self-similarly into an expansion wave is not specific to the screen problem and is likely to occur in other two-dimensional Riemann problems for the compressible Euler equa-

tions and hyperbolic systems of conservation laws. The UTSDE equation provides a universal asymptotic equation for such problems, and therefore the self-similar diffraction of a shock into an expansion wave that disappears at a sonic point is likely to be a generic feature.

A further motivation for this work is to understand the structure of nearly glancing Mach reflections. Lighthill [11] showed that, according to linearized theory, the strength of the reflected shock approaches zero at the triple point in such reflections. Therefore, in order to understand the nonlinear structure of the solution near the triple point, one has to understand how the weak reflected shock diffracts nonlinearly into the Mach shock as its strength approaches zero. A strong Mach shock may be described, in a first approximation, as a "soft" boundary $y = 0$ on which the pressure is constant. This suggests that we study a half-space initial-boundary value problem for (1.1)–(1.2) in $y > 0$ with $u = 0$ on $y = 0$. We show numerical solutions of this IBVP in Section 8.2. The solution has a complex structure, with an apparently infinite sequence of shock-rarefaction reflections, which is similar to what we observe in the Guderley Mach reflection of weak shocks [15].

An outline of the rest of this paper is as follows. In Section 2, we summarize the linearized solution of the wave equation for a self-similar cylindrical wave, including the linearized solution for the screen problem illustrated in Figure 1. In Section 3, we explain how the matching condition (1.2) for the weakly nonlinear solution near S arises from the linearized solution; we also explain why a straightforward dominant balance argument fails to determine the size of the region around S where nonlinearity becomes important. In Section 4, we write out convenient self-similar forms of the UTSDE (1.1). In Section 5, we show that the resulting self-similar equations are themselves self-similar and reduce to an ODE. We also formulate BVPs for the ODE solution behind a shock and an expansion wavefront. It does not, however, appear possible to join solutions of these BVPs smoothly together across $y = 0$, which breaks the second self-similarity of the problem. In Section 6, we approximate these ODE solutions for small α to obtain 'nonlinearized' matching data that is an improvement over the linearized matching data. This improved data allows us to compute numerical solutions in an effective way; we describe our numerical method in Section 7. We present the numerical solutions in Section 8 and conclude with a discussion of the results in Section 9.

2. Linearized solution. Consider a sound wave propagating in two space dimensions whose strength is of the order $0 < \delta \ll 1$. According to the linearized theory of acoustics, the pressure perturbation $p(x, y, t)$ of the sound wave satisfies the wave equation

$$p_{tt} = c_0^2 \Delta p$$

where c_0 is the sound speed of the unperturbed fluid.

Suppose that a sound wave originates from a source located at $(x, y) = (0, 0)$ at $t = 0$ and is self-similar, meaning that $p(x, y, t)$ is a function of $(x/t, y/t)$ only. Let (r, ϕ) denote polar coordinates

$$r = \left(x^2 + y^2\right)^{1/2}, \qquad \tan\phi = \frac{y}{x}. \tag{2.1}$$

The linearized location of the wavefront of the sound wave is then $r = c_0 t$. If $p = p_0$ for $r > c_0 t$, then the asymptotic behavior of a self-similar solution of the wave equation

near the wavefront has the square-root form

$$p \sim p_0 + \delta k(\phi)\sqrt{1 - \frac{r}{c_0 t}} \qquad \text{as } r \to c_0 t^- \text{ with } \phi \text{ fixed.} \tag{2.2}$$

The function $k(\phi)$ describes the angular dependence of the strength of the wave. The diffracted wave generated by the reflection of a step-function pulse by a wedge has the general properties described above, as do linearized solutions of two-dimensional Riemann problems.

Self-similar solutions of the wave equation for the reflection of a pulse by a wedge or screen were obtained by Keller and Blank [8]. For a pulse at normal incidence to a screen, illustrated in Figure 1, the linearized solution for the pressure perturbation p relative to the pressure behind the incident shock is given explicitly by

$$\begin{aligned} p = \delta\sigma(\phi) &- \frac{\delta}{\pi}\arctan\left[\frac{1-\ell}{1+\ell+2\sqrt{2\ell}\sin(\phi/2)}\right] \\ &+ \frac{\delta}{\pi}\arctan\left[\frac{1-\ell}{1+\ell-2\sqrt{2\ell}\sin(\phi/2)}\right]. \end{aligned} \tag{2.3}$$

Here, $\delta = [p]$ is the pressure jump across the incident shock (which is equal to the pressure jump across the reflected shock in the linearized approximation), and we choose $-\pi < \phi < \pi$, $0 \le \arctan z \le \pi$. The similarity variable ℓ in (2.3) is given by

$$\ell = \frac{r}{c_0 t + \sqrt{c_0^2 t^2 - r^2}},$$

and the function σ accounts for the different pressures ahead of the incident shock, behind the incident shock, and behind the reflected shock:

$$\sigma(\phi) = \begin{cases} -1 & \text{if } -\pi < \phi < -\pi/2, \\ 0 & \text{if } -\pi/2 < \phi < \pi/2, \\ 1 & \text{if } \pi/2 < \phi < \pi. \end{cases}$$

The asymptotic behavior of (2.3) as $r \to c_0 t^-$ is given by (2.2) with $p_0 = \delta\sigma$ and

$$k(\phi) = \frac{2}{\pi}\left[\frac{\sin(\phi/2)}{\cos\phi}\right]. \tag{2.4}$$

3. Weakly nonlinear solution and matching conditions. The linearized solution described in the previous section is not uniformly valid at the wavefront $r = c_0 t^-$ since its derivative becomes infinite there. Methods for the systematic construction of matched asymptotic solutions that account for the effect of weak nonlinearities near the wavefront, and which regularize the linearized square-root singularity, were developed in [3, 4, 5, 6, 9, 12]. We briefly outline the results.

Along a ray with an angle ϕ such that $k(\phi) \neq 0$ in (2.2), the diffraction of the wave in the angular direction is negligible to leading order. The nonlinear behavior of the wave near the wavefront is described by a self-similar solution of the cylindrical inviscid Burgers equation in the radial direction [6]. If $k(\phi) > 0$, the wave is compressive and the wavefront consists of a very weak shock wave across which p jumps by an amount of the order δ^2; if $k(\phi) < 0$, the wave is expansive and the wavefront is an expansion wave across which p is Lipschitz continuous and its derivative jumps by an amount

of the order δ^2. Thus, the diffracted wavefront changes from a shock to an expansion near an angle where k changes sign. In particular, this happens when k has a simple pole or a simple zero.

If $k(\phi)$ has a simple pole, at $\phi = 0$ say, then

$$k(\phi) \sim \frac{C}{\phi} \qquad \text{as } \phi \to 0$$

for some constant C. For example, this happens at a singular point such as A in Figure 1. A weakly nonlinear asymptotic solution near such a point was constructed in [3, 4, 9]. In this case, the transverse diffraction of the wave in the angular direction becomes as important as the nonlinear compression or expansion of the wave in the radial direction. A straightforward dominant balance argument shows that, for a linearized wave whose amplitude is of the order δ, the size of the inner region around the singular point where diffraction balances nonlinearity is of the order δ normal to the wavefront and the order $\delta^{1/2}$ along the wavefront [4]. The inner solution near the singular point is described by a self-similar solution of the UTSDE (1.1) with a suitable far-field condition that is obtained from the requirement that the outer expansion of the inner UTSDE solution matches with the inner expansion of the outer linearized solution. Thus, the linearized solution transmits information about the global flow pattern to the local flow near the singular point on the wavefront. Numerical solutions of the resulting IBVP, which show how a plane incident shock joins with a curved diffracted shock and an expansion wave, are given in [7, 13].

If $k(\phi)$ changes sign through a simple zero, at $\phi = 0$ say, then

$$k(\phi) \sim k'(0)\phi \qquad \text{as } \phi \to 0.$$

For example, this happens at the point S in Figure 1. In this case, the wavefront changes continuously from a shock to an expansion wave. The local solution is then described asymptotically by the UTSDE (1.1) with the matching condition (1.2).

To derive the matching condition, we observe from (2.2) that near such a point the linearized solution for the pressure perturbation has the expansion

$$p - p_0 \sim \delta k'(0)\phi\sqrt{1 - \frac{r}{c_0 t}} \qquad \text{as } r \to c_0 t^- \text{ and } \phi \to 0.$$

We rewrite this equation in terms of the inner UTSDE variables defined in the Appendix. Using (10.4)–(10.5), we find that

$$\tilde{u} \sim \alpha \frac{\tilde{y}}{t}\sqrt{-\left(\frac{\tilde{x}}{t} + \frac{\tilde{y}^2}{4t^2}\right)}$$

where

$$\alpha = \left[\frac{(\gamma+1)k'(0)}{2\sqrt{2}}\right]\left(\frac{\delta}{\rho_0 c_0^2}\right).$$

Here, γ is the ratio of specific heats of the compressible fluid. The condition (1.2) then results from matching the outer limit of the inner UTSDE solution with the inner limit of the outer linearized solution, after we drop the tildes. For the screen data (2.4) we have $k'(0) = 1/\pi$, which determines the parameter α in terms of the pressure jump δ across the incident shock.

The matching data (1.2) is invariant under the transonic scaling

$$u \mapsto \frac{u}{\epsilon}, \quad v \mapsto \frac{v}{\epsilon^{3/2}}, \quad x \mapsto \frac{x}{\epsilon}, \quad y \mapsto \frac{y}{\epsilon^{1/2}}, \quad t \mapsto t$$

which leaves (1.1) invariant. As a result, the small parameter α cannot be removed from the problem by rescaling. The invariance of the matching data under transonic scaling explains why we cannot use a straightforward dominant argument to determine the size of the inner region where nonlinearity and diffraction both become important; in fact, a naive argument would suggest — incorrectly — that linear diffraction dominates nonlinearity in arbitrarily small regions about S. We avoid these difficulties here by retaining the leading order behavior of the linearized solution in the matching data, even though it is formally of higher order in the small expansion parameter α than the weakly nonlinear asymptotic solution.

4. Self-similar UTSDE. The problem (1.1)–(1.2) is self-similar, and its solution depends only on the similarity variables

$$\xi = \frac{x}{t}, \qquad \eta = \frac{y}{t}. \tag{4.1}$$

Writing (1.1) in terms of ξ, η, we get

$$\begin{aligned} -\xi u_\xi - \eta u_\eta + \left(\frac{1}{2}u^2\right)_\xi + v_\eta &= 0, \\ u_\eta - v_\xi &= 0. \end{aligned} \tag{4.2}$$

Equation (4.2) is hyperbolic when $u < \xi + \eta^2/4$, corresponding to supersonic flow in a self-similar coordinate frame, and elliptic when $u > \xi + \eta^2/4$, corresponding to subsonic flow. The equation changes type across the sonic line given by

$$\xi + \frac{\eta^2}{4} = u(\xi, \eta). \tag{4.3}$$

In the UTSDE approximation, the inner limits of the self-similar polar coordinates $(c_0 t - r)/r$, ϕ with respect to the original spatial variables are given by

$$\rho = -\left(\xi + \frac{1}{4}\eta^2\right), \qquad \theta = \eta, \tag{4.4}$$

respectively. It is convenient to define corresponding 'radial' and 'angular' velocity components by

$$u = u, \qquad w = -v + \frac{1}{2}\eta u. \tag{4.5}$$

Making the change of variables (4.4)–(4.5) in (4.2), we get

$$\begin{aligned} \rho u_\rho + w_\theta + \left(\frac{1}{2}u^2\right)_\rho - \frac{1}{2}u &= 0, \\ u_\theta - w_\rho &= 0. \end{aligned} \tag{4.6}$$

This transformation preserves weak solutions since it is linear in u and v.

The matching condition (1.2) for the shock-diffraction problem gives

$$u \sim \alpha\theta\sqrt{\rho}, \quad w \sim \frac{2}{3}\alpha\rho^{3/2} \qquad \text{as } \rho \to \infty. \tag{4.7}$$

The asymptotic behavior of w follows from the asymptotic behavior of u and the equation $w_\rho = u_\theta$. In addition, since there is no disturbance ahead of the wave,

$$u = 0, \quad w = 0 \qquad \text{for } \rho \text{ sufficiently large and negative.} \tag{4.8}$$

The data in (4.7) satisfies the linearization of (4.6),

$$\rho u_\rho + w_\theta - \frac{1}{2}u = 0, \qquad u_\theta - w_\rho = 0.$$

It is the linearized UTSDE solution for a diffracted wavefront with a square-root profile that changes continuously from an expansion in $\theta < 0$ to a compression in $\theta > 0$.

The jump conditions for (4.6) for a shock located at $\rho = R(\theta)$ may be written as

$$R + R_\theta^2 + \langle u \rangle = 0, \tag{4.9}$$

$$R_\theta[u] + [w] = 0, \tag{4.10}$$

where $\langle u \rangle$ denotes the average of u on either side of the shock and $[u]$, $[w]$ denote the jump in u, w across the shock.

In summary, the inner problem for the diffraction of a weak shock into an expansion wavefront consists of the self-similar USTDE (4.6) together with the matching conditions (4.7)–(4.8) and the jump conditions (4.9)–(4.10) across any shocks.

5. Similarity solutions. The PDE (4.6) and matching data (4.7) are compatible with similarity solutions in (ρ, θ) of the form

$$u(\rho,\theta) = \alpha^2\theta^2 F\left(\frac{\rho}{\alpha^2\theta^2}\right), \qquad w(\rho,\theta) = \alpha^4\theta^3 G\left(\frac{\rho}{\alpha^2\theta^2}\right). \tag{5.1}$$

Let us attempt to construct a similarity solution of the form (5.1) for the full problem (4.6)–(4.8). Such a solution would necessarily consist of a shock wave in $\theta > 0$ and an expansion wavefront in $\theta < 0$. Writing

$$z = \frac{\rho}{\alpha^2\theta^2},$$

and using (5.1) in (4.6), we find that $F(z)$, $G(z)$ satisfy the ODEs

$$zF' + \left(\frac{1}{2}F^2\right)' - \frac{1}{2}F = \alpha^2\left(2zG' - 3G\right), \tag{5.2}$$

$$G' = 2\left(F - zF'\right), \tag{5.3}$$

where the prime denotes a derivative with respect to z.

From (4.7), the matching condition for (5.2)–(5.3) is

$$F(z) \sim \sqrt{z}, \quad G(z) \sim \frac{2}{3}z^{3/2} \qquad \text{as } z \to \infty. \tag{5.4}$$

In (5.4) we take the positive square root if $\theta > 0$, corresponding to a compression wave, and the negative square root if $\theta < 0$, corresponding to an expansion wave. We also need to impose appropriate conditions at the wavefront.

At an expansion wavefront located at $z = 0$, we require that the solution matches continuously across the wavefront with the unperturbed solution, so that

$$F(0) = 0, \qquad G(0) = 0. \tag{5.5}$$

At a shock wavefront located $z = z_0$, with $u = w = 0$ ahead of the shock, the jump conditions (4.9)–(4.10) imply that

$$F(z_0) = -2z_0\left(1 + 4\alpha^2 z_0\right), \qquad G(z_0) = 4z_0^2\left(1 + 4\alpha^2 z_0\right). \tag{5.6}$$

The entropy condition $F(z_0) > 0$ holds provided that $-1/4 < \alpha^2 z_0 < 0$.

This analysis leads to the following pair of BVPs. For the expansion wave in $\theta < 0$, we get

$$\begin{aligned} &zF' + \left(\frac{1}{2}F^2\right)' - \frac{1}{2}F = \alpha^2\left(2zG' - 3G\right), \\ &G' = 2\left(F - zF'\right), \\ &F(z) \sim \sqrt{z}, \quad G(z) \sim \frac{2}{3}z^{3/2} \qquad \text{as } z \to \infty, \\ &F(0) = 0, \qquad G(0) = 0, \end{aligned} \tag{5.7}$$

for $0 \le z < \infty$, where we take the negative branch of the square root. For the shock wave in $\theta > 0$, we get

$$\begin{aligned} &zF' + \left(\frac{1}{2}F^2\right)' - \frac{1}{2}F = \alpha^2\left(2zG' - 3G\right), \\ &G' = 2\left(F - zF'\right), \\ &F(z) \sim \sqrt{z}, \quad G(z) \sim \frac{2}{3}z^{3/2} \qquad \text{as } z \to \infty, \\ &F(z_0) = -2z_0\left(1 + 4\alpha^2 z_0\right), \qquad G(z_0) = 4z_0^2\left(1 + 4\alpha^2 z_0\right), \end{aligned} \tag{5.8}$$

for $z_0 \le z < \infty$, where we take the positive branch of the square root.

As shown by the numerical solutions, the full solution is not in fact self-similar. This appears to be because the self-similar shock and expansion solutions do not join together smoothly in the limit $z \to \infty$, corresponding to $\theta \to 0^{\pm}$, but we do not investigate the solvability of (5.7)–(5.8) or the compatibility of their solutions any further here. Instead, we use this solution to obtain a nonlinear version of the linearized matching data that agrees with the linearized solution to leading order in α and corrects for the behavior of the solution at the wavefront. We use this improved matching data in our numerical computations.

6. Wavefront expansion. The linearized data (1.2) has a square-root singularity at the wavefront, which is qualitatively incorrect since the nonlinear solution has a discontinuity across a shock and is Lipschitz continuous across an expansion wavefront.

We obtain a 'nonlinearized' solution with the correct qualitative behavior at the wavefront by neglecting the small term on the right-hand side of (5.2), which corresponds to neglecting the term w_θ in the first equation of (4.6). This gives equations that describe the behavior of solutions normal to the wavefront but neglect diffraction effects transverse to the wavefront. Such solutions provide a leading-order approximation to the solution near a wavefront where the coefficient $k(\phi)$ of the linearized

square-root singularity (2.2) does not vanish. It is therefore reasonable to expect that they provide an approximation to the wavefront behavior in the present problem as $\theta \to \infty$ and also more accurate far-field matching data than the linearized data.

Approximating (5.2)–(5.3) to leading order in α^2, we get

$$zF' + \left(\frac{1}{2}F^2\right)' - \frac{1}{2}F = 0, \qquad G' = 2\left(F - zF'\right).$$

The solution of this system subject to the asymptotic condition (5.4) is

$$F(z) = 1 + \sqrt{1+z}, \qquad G(z) = \frac{2}{3}\left[1 + \sqrt{1+z}\,\right]^3 \tag{6.1}$$

where we choose the positive square root for the compression solution in $\theta > 0$ and the negative square root for the expansion solution in $\theta < 0$.

In the case of the negative square root, the functions F, G are given by (6.1) for $0 \le z < \infty$. They vanish at $z = 0$, and we extend them continuously by zero for $-\infty < z < 0$.

In the case of the positive square root, we cannot extend F, G continuously by zero, and we get a discontinuity at some $z = z_0$. The leading order approximation in α of the jump condition (5.6) is

$$F(z_0) = -2z_0, \qquad G(z_0) = 4z_0^2.$$

The approximate shock solution (6.1) satisfies both these conditions if

$$z_0 = -\frac{3}{4}.$$

Thus, the approximate shock-solution is given by (6.1) in $-3/4 < z < \infty$, and by $F = 0$, $G = 0$ in $-\infty < z < -3/4$.

Using (6.1) in (5.1), we find that the corresponding solution for u, w is

$$\begin{aligned} u(\rho,\theta) &= \alpha^2\theta^2 + \alpha\theta\sqrt{\rho + \alpha^2\theta^2}, \\ w(\rho,\theta) &= \frac{2}{3}\alpha\left(\alpha\theta + \sqrt{\rho + \alpha^2\theta^2}\right)^3 \end{aligned} \tag{6.2}$$

where we take the positive square root in both $\theta < 0$ and $\theta > 0$. If $\theta < 0$, then the functions u, w in (6.2) are defined for $0 \le \rho < \infty$ and zero when $\rho = 0$, so we may extend them continuously by zero for $-\infty < \rho < 0$. If $\theta > 0$, then we extend the solutions for u, w by zero on $-\infty < \rho < \rho_0$, where

$$\rho_0 = -\frac{3\alpha^2\theta^2}{4} \tag{6.3}$$

is the approximate shock location. This solution satisfies the jump condition (4.10) exactly, but it satisfies (4.9) only to leading order in α, so the discontinuity in (u, w) is not an exact shock solution.

The asymptotic behavior as $\rho \to \infty$ of the solution (6.2) agrees with the linearized asymptotic behavior (4.7) to leading order in α and ρ. For example,

$$u(\rho,\theta) \sim \alpha\theta\sqrt{\rho} + \alpha^2\theta^2 + O\left(\frac{\alpha^3\theta^3}{\sqrt{\rho}}\right) \qquad \text{as } \rho \to \infty.$$

The higher-order terms in α represent nonlinear corrections to the far-field linearized solution.

For the numerical computations, it is convenient to introduce a potential Φ such that

$$u = \Phi_\rho, \qquad w = \Phi_\theta. \tag{6.4}$$

The potential corresponding to the wavefront data (6.2) is

$$\Phi(\rho,\theta) = \alpha^2\rho\theta^2 + \frac{2}{3}\alpha^4\theta^4 + \frac{2}{3}\alpha\theta\left(\rho + \alpha^2\theta^2\right)^{3/2} \tag{6.5}$$

where we again take the positive branch of the square root. If $\theta < 0$, then Φ is defined for $0 \le \rho < \infty$ and zero with zero derivatives when $\rho = 0$, and we extend it continuously by zero for $-\infty < \rho < 0$. If $\theta > 0$, then the solution (6.5) for the potential is defined in $\rho_0 \le \rho < \infty$ and zero at ρ_0, where ρ_0 is the approximate shock location (6.3), and we extend it continuously by zero for $-\infty < \rho < \rho_0$, although its derivatives jump across $\rho = \rho_0$.

7. Numerical method. The numerical method we use was developed in [15] to solve self-similar problems for the UTSDE. We briefly review the method here (see [15] for a detailed description) and then discuss the boundary conditions used for the present problem.

7.1. Numerical scheme for the UTSDE. We write the UTSDE (1.1) in terms of the self-similar variables used in [15],

$$\begin{aligned} &r = \frac{x}{t} + \frac{y^2}{4t^2}, \qquad \theta = \frac{y}{t}, \qquad \tau = \log t, \\ &\bar{u} = u - r, \qquad \bar{v} = v - \frac{1}{2}\theta u, \end{aligned} \tag{7.1}$$

which gives

$$\begin{aligned} \bar{u}_\tau + \left(\frac{1}{2}\bar{u}^2\right)_r + \bar{v}_\theta + \frac{3}{2}\bar{u} + \frac{1}{2}r = 0, \\ \bar{u}_\theta - \bar{v}_r = 0. \end{aligned} \tag{7.2}$$

These variables are related to the ones introduced in Section 4 by

$$r = -\rho, \qquad \theta = \theta, \qquad \bar{u} = u + \rho, \qquad \bar{v} = -w.$$

To solve (7.2) numerically, we follow the classical Cole-Murman approach. We introduce a potential $\varphi(r,\theta,\tau)$ such that

$$\bar{u} = \varphi_r, \qquad \bar{v} = \varphi_\theta, \tag{7.3}$$

and write the system (7.2) in the scalar form as

$$\varphi_{r\tau} + \left(\frac{1}{2}\varphi_r^2\right)_r + \varphi_{\theta\theta} + \frac{3}{2}\varphi_r + \frac{1}{2}r = 0. \tag{7.4}$$

Equation (7.4) can be solved using standard transonic finite difference techniques. Although this equation is unsteady because of the first term on the left, its solutions

(for self-similar problems) are stationary. We use a high order method, and iterate in time τ until a solution of (7.4) converges to a steady state, using line relaxation. The "pseudo-velocities" $\bar{u}$ and $\bar{v}$ are recovered from the potential in the standard way, and the physical velocity perturbations u and v are then obtained through (7.1). See [14, 15] for full details. For "pseudo-steady" solutions, the potential $\varphi(r,\theta)$ is related to the potential $\Phi(\rho,\theta)$ in (6.4) by

$$\varphi = -\Phi - \frac{1}{2}r^2.$$

7.2. Boundary conditions. We carried out numerical solutions of (7.4) subject to the wavefront-corrected matching data (6.2), which gives

$$\bar{u}(r,\theta) \sim -r + \alpha^2\theta^2 + \alpha\theta\sqrt{-r+\alpha^2\theta^2},$$
$$\bar{v}(r,\theta) \sim -\frac{2}{3}\alpha\left(\alpha\theta + \sqrt{-r+\alpha^2\theta^2}\right)^3$$

as $r \to -\infty$, with

$$\bar{u} = -r, \qquad \bar{v} = 0 \qquad \text{for } r \text{ sufficiently large and positive.}$$

Here, we take the positive branch of the square root throughout. The potential $\varphi(r,\theta)$ corresponding to the potential $\Phi(\rho,\theta)$ in (6.5) is given by

$$\varphi(r,\theta) = \alpha^2 r\theta^2 - \frac{2}{3}\alpha^4\theta^4 - \frac{2}{3}\alpha\theta(-r+\alpha^2\theta^2)^{3/2} - \frac{1}{2}r^2.$$

In $\theta < 0$, we use this potential for $-\infty < r \le 0$ and extend it continuously by $-r^2/2$ (corresponding to $u = v = 0$) for $0 < r < \infty$. In $\theta > 0$, we use this potential for $-\infty < r \le 3\alpha^2\theta^2/4$ and extend it continuously by $-r^2/2$ for $3\alpha^2\theta^2/4 < r < \infty$. This gives an approximate solution of the UTSDE that corrects the behavior of the linearized solution near the expansion wavefront or shock, and has the same asymptotic behavior as $r \to -\infty$ as the linearized solution to leading order in α.

On the outer numerical boundaries we impose Dirichlet data corresponding to this wavefront potential and its extension as described above. Specifically, we impose as a numerical boundary condition

(7.5)
$$\varphi(r,\theta) = \begin{cases} \alpha^2 r\theta^2 - \frac{2}{3}\alpha^4\theta^4 - \frac{2}{3}\alpha\theta(-r+\alpha^2\theta^2)^{3/2} - \frac{1}{2}r^2, & \theta < 0, r \le 0, \\ -r^2/2, & \theta < 0, r > 0, \\ \alpha^2 r\theta^2 - \frac{2}{3}\alpha^4\theta^4 - \frac{2}{3}\alpha\theta(-r+\alpha^2\theta^2)^{3/2} - \frac{1}{2}r^2, & \theta > 0, r \le 3\alpha^2\theta^2/4, \\ -r^2/2, & \theta > 0, r > 3\alpha^2\theta^2/4. \end{cases}$$

8. Numerical results. In this section we show numerical solutions of the diffraction problem (1.1)–(1.2) and a related half-space problem. As explained in the previous section, we obtained these solutions by solving the transformed equations (7.4)–(7.5), then plotting u as a function of the similarity variables $(x/t, y/t)$.

8.1. The diffraction problem. We computed numerical solutions of (1.1)–(1.2) for α equal to 0.01, 0.05, 0.1, 0.2, 0.3, 0.4, and 0.45. In the following figures, we show solutions for the values 0.1, 0.2, and 0.3. The solutions for the other values of α are similar to the ones presented here.

Figure 2 shows u-contour plots of the global solution, and illustrates the computational domain used. The left and right boundaries of the computational domain

are curved because of the use of the parabolic coordinate r in (7.1). The dashed line in these plots is the numerically computed location of the sonic line (4.3), and the u-contour levels are indicated on the plots. The solution is subsonic to the left of the sonic line and supersonic to the right.

The numerical solutions depicted in Figure 2 are all qualitatively similar. There is a shock wavefront located on the sonic line for $y/t = \theta$ larger than some particular negative value (depending on α) of θ, which we will denote by $\theta_*(\alpha)$, and an expansion wavefront for smaller values of θ. The shock appears to die out and become an expansion at the sonic line. (We refer to the locus of transition points between supersonic and subsonic flow as the sonic line, whether the flow is continuous there or not.) Values of u jump from 0 to positive values as the shock is crossed from right to left in the direction of flow, and values of u decrease smoothly from 0 to negative values as the expansion wavefront is crossed from right to left. The shock wavefront becomes stronger as α increases, and the expansion wave also increases in strength with increasing α. For a fixed value of α, the shock increases in strength as θ increases. The plots in Figure 2 show that the shock wavefront moves further to the right in x/t as α increases. This is due to the boundary condition (7.5), which shows that the shock location (at a given value of θ) is proportional to α^2.

In the numerical solutions depicted in Figure 2, the transition between the shock and expansion wavefront takes place continuously at a value of y/t equal to $\theta_*(\alpha)$. In order to show this continuous transition more clearly, in Figure 3 we show surface plots of u as a function of $(x/t, y/t)$. The point at which the shock dies out, reaches zero strength, and becomes an expansion wavefront is clearly visible in these plots. From the plots, the value of $y/t = \theta_*(\alpha) < 0$ where this occurs, becomes more negative as α increases, meaning that the shock diffracts further into the expansion region as the wave gets stronger. For example, from the numerical solutions, $\theta_*(0.1) \approx -0.7$ while $\theta_*(0.3) \approx -2.1$.

In the plots in Figure 2 and Figure 3, the shock appears to die out on the sonic line. To determine if the shock reaches zero strength exactly at the sonic line (and not at a point inside the supersonic region), we computed a highly refined solution of (7.4)-(7.5) for α equal to 0.3, using a nonuniform grid with a locally refined area of uniform grid surrounding the apparent shock die-out point. Figure 4 shows u-contours and the sonic (dashed) line near the point at which the shock reaches zero strength. In this solution we used approximately 17×10^6 points, of which 9×10^6 points were devoted to the local refinement. The u-contour with value $u = 0$ is indicated on the plot; above this contour, the shock has non-zero strength. As shown, the shock appears to reach zero strength exactly on the sonic line. The small numerical oscillations immediately behind the shock near the point where it dies out seem to be caused by the use of a stretched grid.

In order to determine the functional relationship between the y/t location where the shock dies out and α, in Figure 5 we plot $\theta_*(\alpha)$ as a function of α using the numerically determined values of θ_* from all of the numerical solutions we obtained. In this figure, the numerical data pairs (α, θ_*) are plotted as symbols. We fit the numerical data to the following curve:

$$-\theta_*(\alpha) = 5\alpha^2 + 5.75\alpha. \tag{8.1}$$

This curve is plotted as a solid line in the figure, and appears to model the data fairly well. From the data and the curve (8.1), we see that $\theta_* \to 0$ as $\alpha \to 0$.

As a check on the numerical computations, we plotted the shock strength $[u]$ as a function of the distance $\theta - \theta_*$ from the point where the shock dies out. The plot

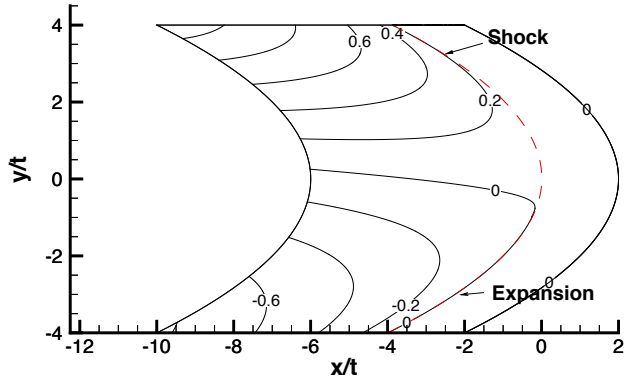

(**a**) $\alpha = 0.1$

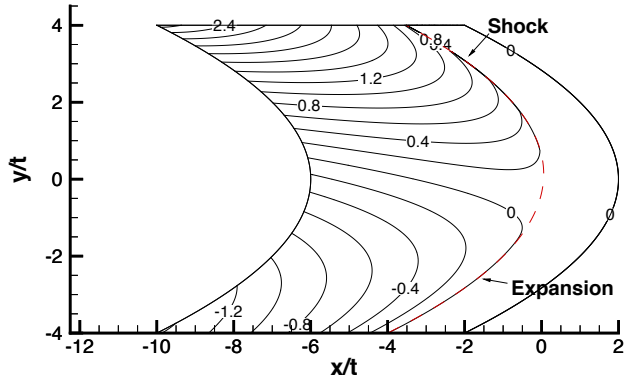

(**b**) $\alpha = 0.2$

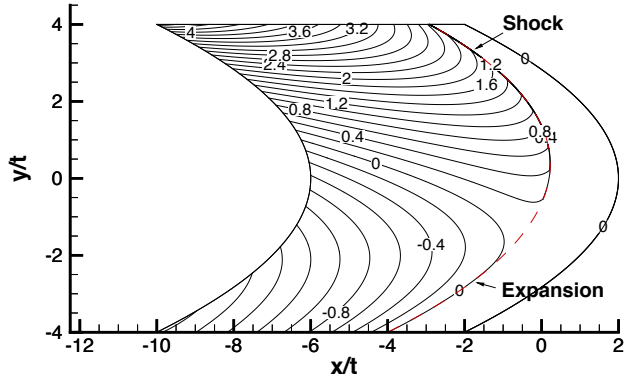

(**c**) $\alpha = 0.3$

FIG. 2. *Contour plots of u over the full numerical domain, for increasing values of α. The u-contour spacing, as indicated by the displayed values of u, is 0.2. The dashed red line is the sonic line; flow to the right of the sonic line is supersonic, and flow to the left of it is subsonic. The solutions in (a), (b) and (c) were computed on uniform grids which contain 1000×1000 grid points.*

from the numerical solution with $\alpha = 0.4$ is shown in Figure 6. The shock strength data were obtained from the numerical solution at the locations indicated by the data

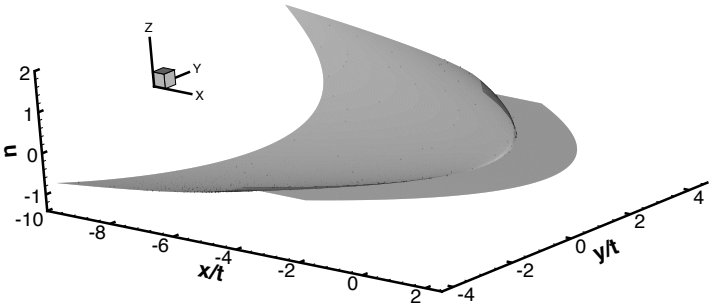

(**a**) $\alpha = 0.1$

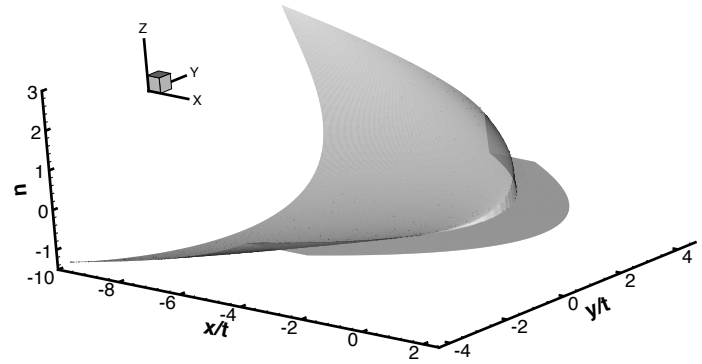

(**b**) $\alpha = 0.2$

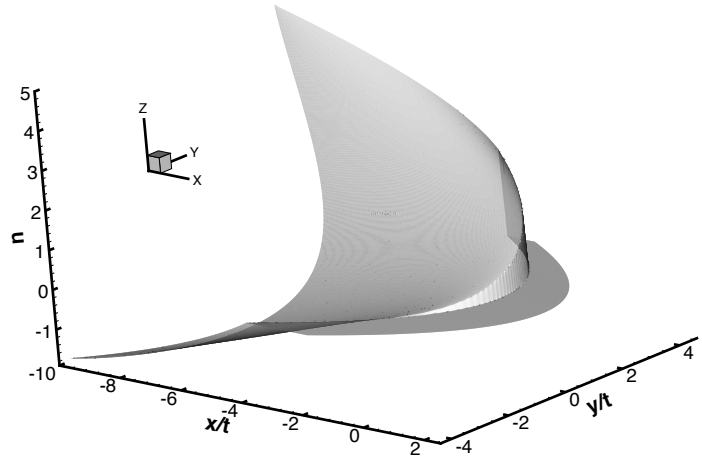

(**c**) $\alpha = 0.3$

FIG. 3. *Plots of the function $z = u(x/t, y/t)$ for the three solutions displayed in Figure 2(a–c). The nearly discontinuous jump in u in each of the plots in (a)–(c) is the numerical shock. The values of u smoothly decrease across the expansion wavefront.*

points in the plot by taking cross-sections of u normal to the shock. We then fit the

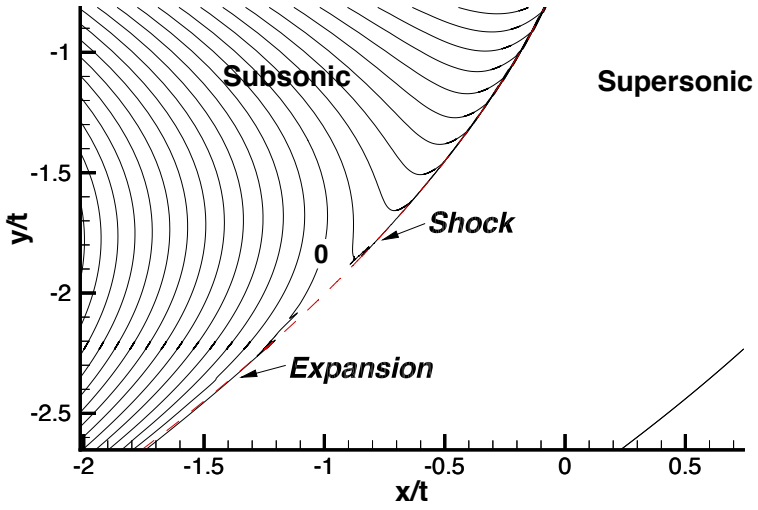

FIG. 4. *A plot of u-contours near the point where the shock becomes an expansion. The dashed (red) line is the sonic line. The u-contour spacing is* 0.015. *The curve visible in the lower right is part of the outer numerical boundary. The region shown contains the refined uniform grid, which has* 3000×3000 *grid points* ($\Delta(x/t) = \Delta(y/t) = 1 \times 10^{-5}$).

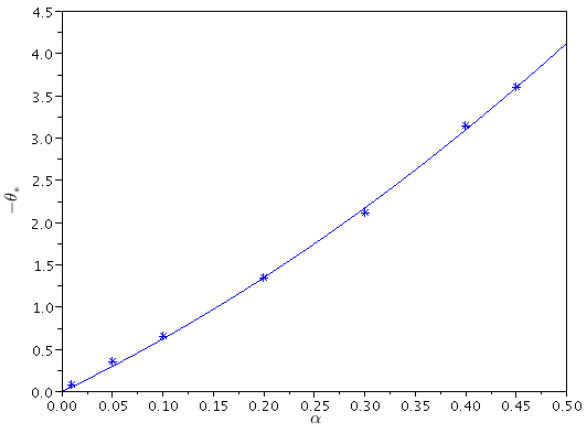

FIG. 5. *The* y/t *location* θ_* *of the point where the shock becomes an expansion, as a function of* α. *The data from the numerical solutions are plotted as symbols. The solid curve is equation (8.1).*

data to the curve

$$[u] = 0.08(\theta - \theta_*)^2, \tag{8.2}$$

which is plotted as a solid line in the figure, and which appears to fit the data well. In Section 9, we compare this to a theoretical result and discuss the implications for our numerical solutions.

8.2. The half-space problem. In addition to the solutions just presented, we computed a solution of a problem for (7.4)–(7.5) on the half space $y/t > 0$, with the

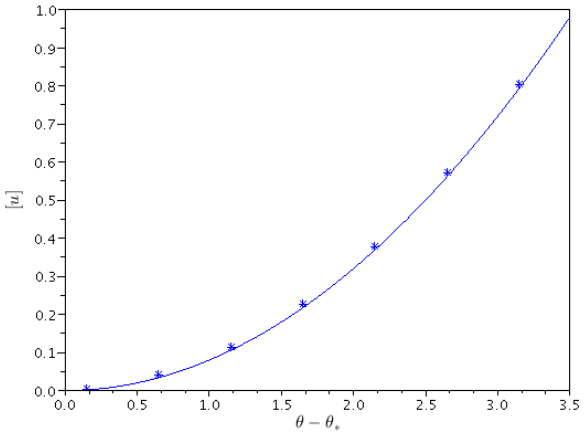

FIG. 6. *The behavior of shock strength with distance from the point where the shock dies out, $\theta - \theta_*$ (from the numerical solution with $\alpha = 0.4$). The data from the numerical solution are plotted as symbols, and the solid curve is equation (8.2).*

boundary condition

$$u = 0 \qquad \text{on } y/t = 0. \tag{8.3}$$

For this problem, we imposed only the part of the matching data in (7.5) for $y/t > 0$. The condition (8.3) corresponds physically to a "soft" boundary on which the pressure is constant. We chose this problem because of its relationship to the problem of weak shock reflection off a wedge [15]; a "soft" boundary provides a model for the reflection of a weak diffracted shock off a strong Mach shock at a triple point.

Figure 7(a)–(b) shows u-contour plots of the solution of this zero-pressure boundary problem, obtained with $\alpha = 0.3$. The red line in these plots is the sonic line. The plot in (a) shows the full global solution, and illustrates the computational domain used — just the upper half of the computational domain used in the solutions shown above. On the top, left and right computational boundaries, we imposed the wavefront data (7.5). On the lower boundary $y/t = 0$ we imposed (8.3), which implies that $\varphi = -r^2/2$ on $y/t = 0$. The plot in (a) shows a shock wavefront reflecting off the "soft" boundary $y/t = 0$. We used local grid refinement in a neighborhood surrounding this reflection point, and an enlargement of the solution near the reflection point is shown in (b). In a tiny area behind the reflection point, there is a supersonic patch that is formed by a sequence of weak shocks and expansions that reflect between the sonic line and the lower boundary. This structure closely resembles a Guderley Mach reflection (GMR), which we have found in problems for weak shock reflection (see [15, 16, 17]). In Section 9, we compare the solution shown in Figure 7(b) to GMR and elaborate on this resemblance.

We note that, in computing the solutions shown in Figure 4 and Figure 7, we used grid continuation, in which partially converged coarse grid solutions are interpolated onto more refined grids and converged on the refined grids. In both of these computations, we performed successive grid refinements until further refinement of the grid resulted in no observable change in the solution. Thus, in the solution shown in Figure 4, the computation was stopped when no further change in the position of the shock die-out point was observed, an indication of grid convergence. Similarly,

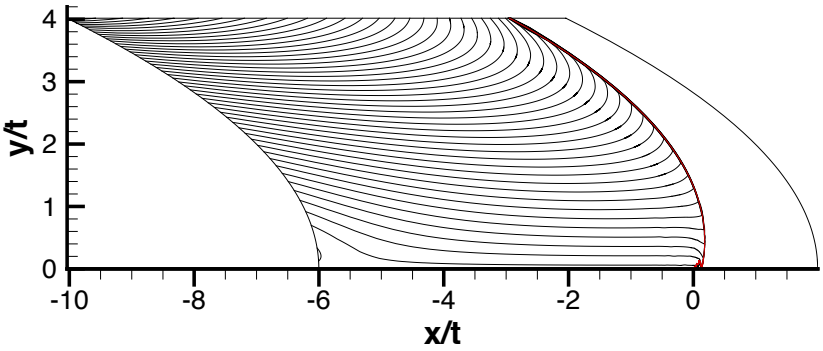

(a)

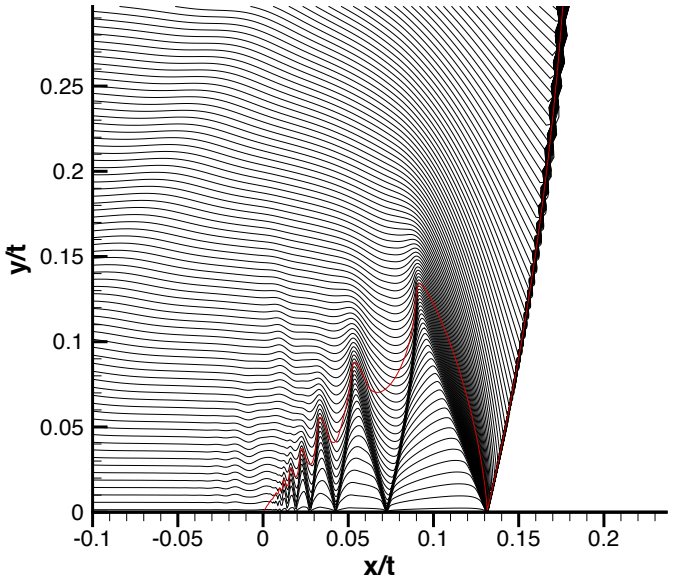

(b)

FIG. 7. *Contour plots of u for the numerical solution of the zero-pressure boundary problem (7.4)-(7.5),(8.3). The plot in (a) shows the solution over the full numerical domain. The shock reflects off the boundary $y/t = 0$. The plot in (b) shows a closeup near the reflection point. The red line in these plots is the sonic line. The u-contour spacing is 0.1 in (a), and 0.003 in (b). In these plots, the flow is supersonic to the right of the sonic line and subsonic to the left. The full grid in (a) contains* 2670×2100 *grid points. The region shown in (b) contains the refined uniform grid, which has* 1500×1500 *grid points* ($\Delta(x/t) = \Delta(y/t) = 1 \times 10^{-4}$).

the solution shown in Figure 7 was determined to be grid converged when one further refinement of the grid produced almost no observable change in the details of the GMR structure.

9. Interpretation of the numerical results. A significant feature of the numerical solutions of the shock diffraction problem (7.4)–(7.5) is that the shock appears to die out exactly at the sonic line. This sonic shock disappearance point is shown clearly in Figure 4. Our use of a grid continuation procedure, with grid refinement continuing until evidence of grid convergence is obtained, suggests that the picture of

the disappearance of a shock at the sonic line is not likely to change under further grid refinement. The disappearance of a diffracting shock at a sonic point contrasts with the formation of a shock at a supersonic point due to coalescence of compression waves that are reflected from a sonic line, as originally proposed by Guderley [2] and recently confirmed in the computations in [14].

We next use the wavefront solution (6.2), which we impose as a numerical boundary condition in our computations, to explain our result in Figure 6. According to (6.2), on $\rho = 0$ we have

$$u = \begin{cases} 2\alpha^2\theta^2, & \theta > 0, \\ 0, & \theta < 0. \end{cases}$$

Ahead of the shock, whose approximate location is given by (6.3), $u = 0$. Therefore, the shock strength $[u]$ in the wavefront solution is proportional to θ^2, and the shock strength $[u] \to 0$ as $\theta \to 0$. This is consistent with the numerical result depicted in Figure 6, with θ^2 replaced by $(\theta - \theta_*)^2$. (In the numerical solutions, the shock diffracts into the expansion wavefront and reaches zero strength at $\theta = \theta_*$ instead of at $\theta = 0$, and so the shock strength $[u]$ is proportional to $(\theta - \theta_*)^2$ instead of θ^2.) This agreement between the numerical solution and the approximate wavefront solution provides a check on the accuracy of the numerical method.

There is a close relationship between the solution of the zero-pressure boundary condition problem (7.4)–(7.5),(8.3), shown in Figure 7, and Guderley Mach reflection solutions of weak shock reflection problems that we have previously obtained. To illustrate this close relationship, Figure 8 shows a solution of the weak shock reflection problem for the UTSDE obtained in [15]. The plots in Figure 7(b) and Figure 8 both show u-contours and the numerically computed location of the sonic line in a tiny region behind the reflection point. Both solutions contain a sequence of weak shocks and expansion waves that are reflected between a sonic line and a lower boundary, with the shocks reflecting off the lower boundary as expansion waves, and the expansion waves reflecting off the sonic line as compression waves which form shocks. In the zero-pressure boundary problem, the lower boundary (at $y/t = 0$) is "soft,", while in the GMR solution in Figure 8 the lower boundary is the Mach stem. Hence, in the GMR solution the points at which the shock reflects off the lower boundary are shock triple points. Guderley [2] argued that the sonic line must pass exactly through a triple point in the case of steady shock reflection, but it is not clear that this must be exactly true in the self-similar case. Nevertheless, in our previous numerical solutions of self-similar GMR (see [15, 16, 17]), the sonic line does appear to pass through the first several triple points in the sequence, as shown in Figure 8. In addition, in these solutions the sonic line approached the triple points more and more closely as the grid resolution was increased. This contrasts with the situation shown in Figure 7(b). There, although the sonic line passes directly through the first reflection point, it does not even approximately pass through the rest, and this does not appear to be a result of inadequate numerical resolution. Further investigation is required to determine whether or not the secondary triple points in this reflection off a soft boundary have a different sonic structure from those in a GMR off a rigid boundary.

10. Appendix: the UTSDE. In this appendix, we briefly summarize the derivation of the UTSDE equation for compressible flows. For more details and further discussion, see *e.g.* [1, 4, 18].

The density ρ, pressure p, and velocity $\mathbf{u} = (u, v)$ of an inviscid, compressible fluid in two space dimensions, with Cartesian coordinates $\mathbf{x} = (x, y)$, satisfy the

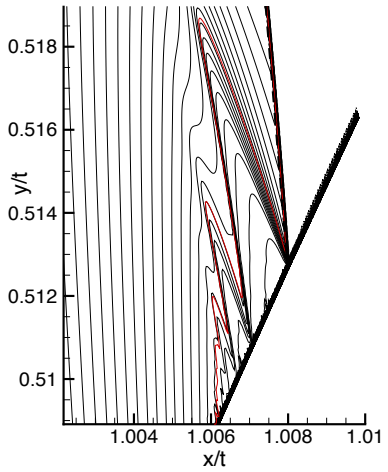

FIG. 8. *Guderley Mach reflection (GMR), as obtained in [15]. The plot shows u-contours; the red line is the sonic line. The u-contour spacing is 0.003. The flow is supersonic to the right of the sonic line and subsonic to the left.*

compressible Euler equations

$$\begin{aligned} &\rho_t + \nabla \cdot (\rho \mathbf{u}) = 0, \\ &(\rho \mathbf{u})_t + \nabla \cdot (\rho \mathbf{u} \otimes \mathbf{u} + p) = 0, \\ &\left(\rho \left[e + \frac{1}{2}\rho \mathbf{u}^2\right]\right)_t + \nabla \cdot \left(\rho \left[e + \frac{1}{2}\rho \mathbf{u}^2\right] \mathbf{u}\right) = 0, \end{aligned} \tag{10.1}$$

where e is the specific internal energy of the fluid. For definiteness, we consider an ideal gas with constant ratio of specific heats $\gamma > 1$ and equation of state

$$e(p, \rho) = \left(\frac{1}{\gamma - 1}\right) \frac{p}{\rho},$$

but the same analysis applies to a general equation of state.

The UTSDE asymptotic expansion for a weakly nonlinear sound wave propagating in the x-direction and diffracting more slowly in the y-direction is

$$\begin{aligned} \begin{pmatrix} \rho \\ u \\ v \\ p \end{pmatrix} = \begin{pmatrix} \rho_0 \\ 0 \\ 0 \\ p_0 \end{pmatrix} &+ \epsilon U \left(\frac{x - c_0 t}{\epsilon}, \frac{y}{\epsilon^{1/2}}, t\right) \begin{pmatrix} \rho_0 \\ c_0 \\ 0 \\ \rho_0 c_0^2 \end{pmatrix} \\ &+ \epsilon^{3/2} V \left(\frac{x - c_0 t}{\epsilon}, \frac{y}{\epsilon^{1/2}}, t\right) \begin{pmatrix} 0 \\ 0 \\ c_0 \\ 0 \end{pmatrix} + O(\epsilon^2), \end{aligned} \tag{10.2}$$

where ρ_0, p_0 are the unperturbed density and pressure, respectively, $c_0 = \sqrt{\gamma p_0 / \rho_0}$ is the unperturbed sound speed, and $0 < \epsilon \ll 1$ is small positive parameter that measures the amplitude of the wave and the size of its x and y derivatives. The scaling chosen in (10.2), with $u = O(\epsilon)$, $\partial_x = O(\epsilon^{-1})$, $\partial_y = O(\epsilon^{-1/2})$ after a suitable

nondimensionalization, is the one that leads to a dominant balance between weak nonlinearity and weak diffraction on a time-scale of the order 1.

Use of the expansion (10.2) in the compressible Euler equations (10.1) implies that $U(X,Y,t)$, $V(X,Y,t)$ satisfy the UTSDE equation

$$\begin{aligned} &U_t + \left(\frac{\gamma+1}{4}c_0U^2\right)_X + \frac{1}{2}c_0V_Y = 0,\\ &U_Y - V_X = 0. \end{aligned}$$

Introducing normalized variables

$$\begin{aligned} &\tilde{u} = \left(\frac{\gamma+1}{2}\right)U, \qquad \tilde{v} = \left(\frac{\gamma+1}{2\sqrt{2}}\right)V,\\ &\tilde{x} = \frac{X}{c_0}, \qquad \tilde{y} = \frac{\sqrt{2}Y}{c_0}, \end{aligned} \tag{10.3}$$

we find that $\tilde{u}(\tilde{x},\tilde{y},t)$, $\tilde{v}(\tilde{x},\tilde{y},t)$ satisfy

$$\begin{aligned} &\tilde{u}_t + \left(\frac{1}{2}\tilde{u}^2\right)_{\tilde{x}} + \tilde{v}_{\tilde{y}} = 0,\\ &\tilde{u}_{\tilde{y}} - \tilde{v}_{\tilde{x}} = 0, \end{aligned}$$

which is (1.1), after we drop the tildes.

For the matching, it is useful to note how polar coordinates (r,ϕ) with respect to the original spatial variables, given in (2.1), transform into the asymptotic variables. As $\epsilon \to 0^+$ with $\tilde{x}$, $\tilde{y}$, t fixed, we have

$$\frac{r-c_0t}{c_0t} \sim \epsilon\left[\frac{\tilde{x}}{c_0t} + \frac{\tilde{y}^2}{4t^2}\right] \qquad \phi \sim \frac{\epsilon^{1/2}}{\sqrt{2}}\frac{\tilde{y}}{t}. \tag{10.4}$$

Moreover, the pressure perturbation is related to $\tilde{u}$ by

$$p - p_0 \sim \epsilon\rho_0c_0^2\left(\frac{2}{\gamma+1}\right)\tilde{u}. \tag{10.5}$$

REFERENCES

[1] J. D. Cole and L. P. Cook, *Transonic Aerodynamics*, Elsevier, Amsterdam, 1986.

[2] K. G. Guderley, *The Theory of Transonic Flow*, Pergamon Press, 1962.

[3] E. Harabetian, *Diffraction of a weak shock by a wedge*, Comm. Pure Appl. Math., 40 (1987), pp. 849–863.

[4] J. K. Hunter, *Transverse diffraction of nonlinear waves and singular rays*, SIAM J. Appl. Math., 48 (1988), pp. 1–37.

[5] J. K. Hunter and M. Brio, *Weak shock reflection*, J. Fluid Mech., 410 (2000), pp. 235–261.

[6] J. K. Hunter and J. B. Keller, *Weak shock diffraction*, Wave Motion, 6 (1984), pp. 79–89.

[7] J. K. Hunter and A. M. Tesdall, *Weak shock reflection*, in A Celebration of Mathematical Modeling, D. Givoli, M. Grote, and G. Papanicolaou, eds., Kluwer Academic Press, New York, 2004, pp. 93–112.

[8] J. B. Keller and A. Blank, *Diffraction and reflection of pulses by wedges and corners*, Comm. Pure Appl. Math., 4 (1951), pp. 75–94.

[9] J. B. Keller and L. Ting, *Weak diffracted shocks near singular rays*, Methods Appl. Anal., 7 (2000), pp. 565–576.

[10] M. Li and Y. Zheng, *Semi-hyperbolic patches of solutions of the two-dimensional Euler equations*, to appear in Arch. Rat. Mech. Anal..

[11] M. J. Lighthill, *The diffraction of blast. II*, Proc. R. Soc. Lond. A, 200 (1950), pp. 554–565.
[12] C. S. Morawetz, *Potential theory for the regular and Mach reflection of a shock at a wedge*, Comm. Pure Appl. Math., 38 (1994), 593–624.
[13] E. G. Tabak and R. R. Rosales, *Focusing of weak shock waves and the von Neumann paradox of oblique shock reflection*, Phys. Fluids, 6 (1994), pp. 1874–1892.
[14] A. M. Tesdall, *High resolution solutions for the supersonic formation of shocks in transonic flow*, Journal of Hyperbolic Differential Equations, to appear.
[15] A. M. Tesdall and J. K. Hunter, *Self-similar solutions for weak shock reflection*, SIAM J. Appl. Math., 63 (2002), pp. 42–61.
[16] A. M. Tesdall, R. Sanders, and B. L. Keyfitz, The triple point paradox for the nonlinear wave system, *SIAM J. Appl. Math.*, 67 (2006), pp. 321–336.
[17] A. M. Tesdall, R. Sanders, and B. L. Keyfitz, Self-similar solutions for the triple point paradox in gasdynamics, *SIAM J. Appl. Math.*, 68 (2008), pp. 1360–1377.
[18] Y. Zheng, *Systems of Conservation laws: Two Dimensional Riemann Problems*, Birkhäuser, Boston, 2001.